*36th EPS Conference on Plasma Phys. Sofia, June 29 - July 3, 2009 ECA Vol.**33E**, P-2.164 (2009)*

Comparison of divertor power loads with and without TF ripple in JET

H. Thomsen[1], S. Devaux[1], T. Eich[1], G. Arnoux[2], E. de la Luna[3],
W. Fundamenski[2], G.Saibene[4], R. Sartori[4], and JET-EFDA contributors *
JET-EFDA, Culham Science Centre, Abingdon, OX14 3 DB, UK
[1] *Max-Planck-Institut für Plasmaphysik, EURATOM-Assoziation, Greifswald, Germany*
[2] *UKAEA/EURATOM Fusion Association, Abingdon, OX14 3 DB, UK*
[3] *Laboratorio Nacional de Fusion, Association EURATOM-CIEMAT, Madrid, Spain*
[4] *Fusion For Energy Joint Undertaking, Barcelona, Spain*
* *See Appendix of F. Romanelli et al., OV*$/1-2$*, Proceedings of the 22nd IAEA FEC, Geneva, Switzerland (2008)*

Introduction

ITER will operate at a toroidal field (TF) ripple of $\delta_{\mathrm{BT}} \approx 0.5\%$, whereas the natural TF ripple in JET is $\delta_{\mathrm{BT}} = 0.08\%$. Previous identity experiments in JET and JT-60U with toroidal field ripple at the plasma separatrix similar to that expected in ITER indicate that the H-mode plasma confinement degrades and toroidal plasma rotation is decreased [1, 2]. The effect of TF ripple on the H-mode confinement is found to be more pronounced for high plasma current and magnetic field. Here, we concentrate on the impact of the TF ripple on edge localized modes (ELMs) for an unfueled three step ripple scan at the highest toroidal field compatible with ripple operation in JET with $B_t = 2.3T$, $I_{\mathrm{pla}} = 2.6\,\mathrm{MA}$ and $q_{95} = 3.1$.

The NBI-heating was adapted to keep the absorbed power in the plasma approximately constant ($P_{\mathrm{NBI}} = 15\,\mathrm{MW}$ for the natural TF ripple in JET of $\delta_{\mathrm{BT}} = 0.08\%$ to $P_{\mathrm{NBI}} = 18\,\mathrm{MW}$ for $\delta_{\mathrm{BT}} = 0.75\%$). A new infrared camera (FLIR, 14bit, 3-5 μm wavelength range) was used to characterize the power load in the divertor. The camera view was adjusted to record both the inner and the outer strike-line on the target plates, with a resolution < 5 mm and < 2 mm, respectively. The time resolution was 85μs (40μs exposure time) for 10 s recording length. The temperature measurements are converted into heat fluxes with the THEODOR code [3]. Non-uniform carbon layers are taken into account on the outboard divertor target in order to improve the accuracy of the thermographic results on fast (ELM) time scales [4, 5]. Due to the limited resolution, this procedure is not possible for the inboard side, causing a higher uncertainty for the respective data. Semi-automatic software codes were applied in order to determine the start and end of individual ELMs. Based on this information, the time series of power flux profiles on the inner and outer divertor tiles are split into individual ELM and inter-ELM phases which can be used for further statistical analysis.

Results

The three discharges of the scan show a density pump-out effect. The pedestal density decreases linearly from $n_{e,ped} = 5.6\,(\pm 0.2)$ to $n_{e,ped} = 4.4\,(\pm 0.2) \cdot 10^{19} m^{-3}$, whereas the pedestal temperature is approximately constant in the range of $1.5\,(\pm 0.1)$ keV. The average ELM frequency rises with TF ripple, from $f_{ELM}(\delta_{BT} = 0.08\,\%) \approx 22\,Hz$ over $f_{ELM}(\delta_{BT} = 0.5\,\%) \approx 30\,Hz$ to $f_{ELM}(\delta_{BT} = 0.75\,\%) \approx 52\,Hz$. The increase in ELM-frequency with increasing TF ripple was reported in [1, 2]. Typical heatflux profiles on the divertor targets during type-I ELMy H-mode are shown in Fig. 1. The natural TF ripple reference discharge displays phases of compound ELMs.

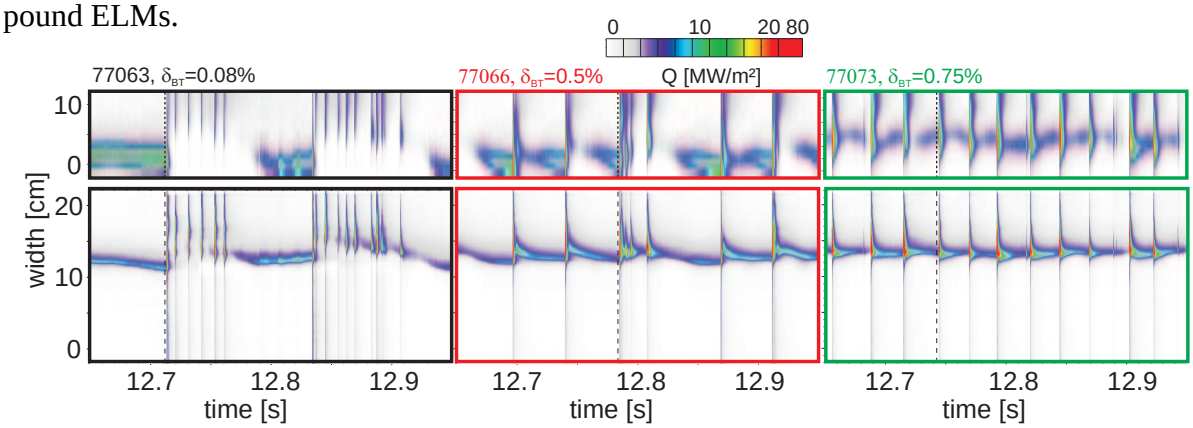

Figure 1: Heat flux profiles of inboard (top) and outboard divertor target (bottom) versus time. The maximum heat flux is limited to 20 MW/m^2 in the plot in order to enhance the visibility of the inter-ELM heatflux.

The pedestal collisionality $\nu^* \approx 0.1$ shows only little variation, cf. Fig 2(a). The $\Delta W_{ELM}/W_{ped}$ for the discharge with $\delta_{BT} = 0.75\%$ are lower than expected from the ν^*-scaling for discharges with natural ripple [6], indicating the reduction of ELM size with TF ripple for similar ν^* [1]. In absolute numbers $\Delta W_{ELM} < 200\,kJ$, approximately 50% below the usual ELM size with natural ripple in JET. It was found that the reduction of the ELM energy loss is caused by a reduced drop of the prompt relative pedestal temperature [1].

The fraction of the ELM energy measured at the target $\Delta W_{target}/\Delta W_{ELM}$ decreases with increasing normalized ELM size, $\Delta W_{ELM}/\Delta W_{ped}$, cf. Fig 2(b). This effect was previously reported for JET discharges with natural TF ripple in [6, 7]. Due to the limited view of the IR camera a considerable fraction of the ELM-deposited power on the inner divertor target cannot be observed, leading to a systematic under-estimation of the total ELM energy.

In Fig. 3 the time averaged power loads during a steady state discharge phase of 4 s are plotted versus δ_{BT}. The plotted error bars represent uncertainties from the inter-ELM contribution during an ELM [7]. The ELM power load in the observed areas of the divertor tiles is increasing with increasing ripple. Also, the inter-ELM power load on the outboard divertor target shows a slight increase, but the inter-ELM power load on the inboard side is decreasing.

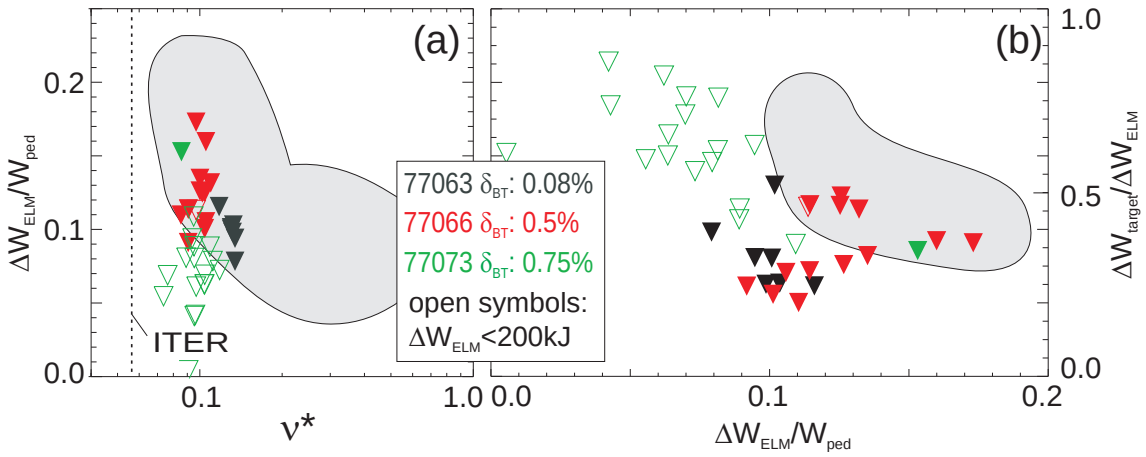

Figure 2: (a) ELM energy loss ΔW_{ELM} normalized to the pedestal energy W_{ped} versus pedestal plasma collisionality. The grey area indicates the operational space covered in [6] for JET discharges with natural TF ripple; the vertical dashed line denotes the expected ITER pedestal plasma collisionality. (b) ELM energy $\Delta W_{\mathrm{target}}$ measured at the divertor by the IR camera, normalized to the diamagnetic energy loss ΔW_{ELM} versus ΔW_{ELM} normalized to the pedestal energy W_{ped}. The grey area indicates the operational space covered in [7] for JET discharges with natural TF ripple.

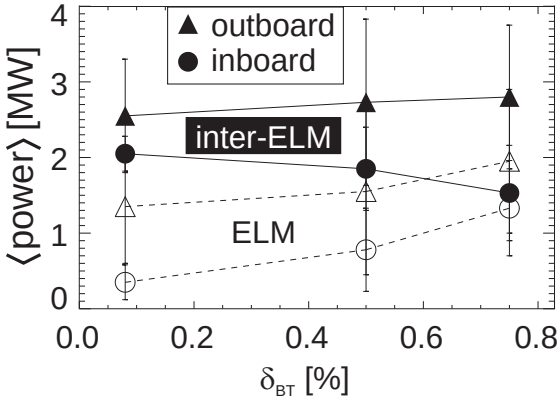

Figure 3: ELM (open symbols) and inter-ELM (filled symbols) time averaged power loads for inner (circle) and outer divertor targets (triangle) as measured by the IR camera versus TF ripple δ_{BT}. $\langle P_{\mathrm{ELM}}\rangle = (\Delta t)^{-1}\int P_{\mathrm{ELM}}\mathrm{d}t$ (with $P_{\mathrm{ELM}} = 0$ during inter-ELM phases) for $\Delta t = 4\,\mathrm{s}$ and analogous for $\langle P_{\mathrm{inter-ELM}}\rangle$.

We find a linear relationship between the outboard ELM power $P_{\mathrm{peak}}^{\mathrm{outer}}$ and the ELM size ΔW_{ELM} at the outboard divertor target, cf. Fig. 4(a). The ELM wetted area in Fig. 4(b) shows a non-linear increase with ΔW_{ELM}. The inter-ELM power and wetted area are almost constant at the outboard divertor target.

Discussion

One important question is the effect of the TF ripple on the ELM dynamics, which is determined by the physics in the scrape-off layer and the pedestal physics. Increasing the TF ripple results in more frequent but smaller ELMs. The ELM-induced power load on the divertor target is increasing, whereas the inter-ELM target power load decreases and the respective inboard-outboard asymmetry intensifies towards the low field side leg. With the current camera setup

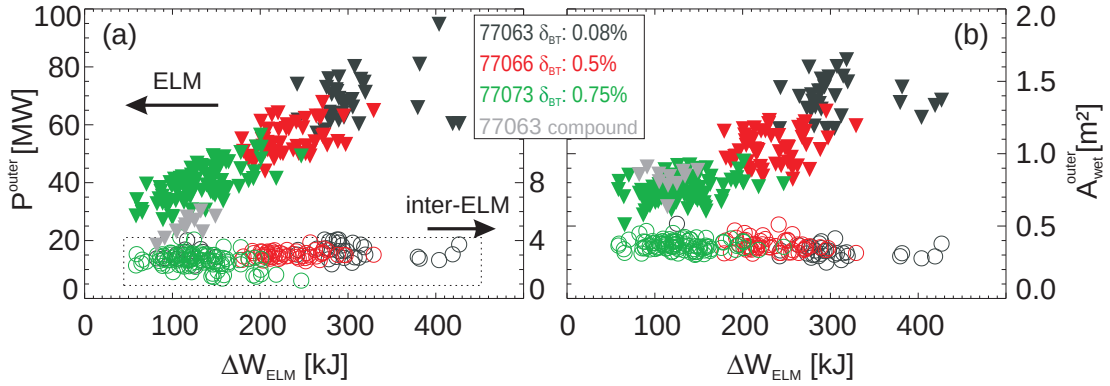

Figure 4: (a) inter-ELM and ELM peak power and (b) wetted area (P/Q) both for the outboard divertor target versus ELM size ΔW_{ELM}. Triangles: ELMs, circles: inter-ELM 1 ms before ELM.

a statement about the inboard-outboard asymmetry of the ELM power load is not possible due to the limited view on the inboard target. The observed inboard ELM power load increase with TF ripple is presumably caused by a reduced wetted area. For the outboard divertor target, such a decrease of the ELM wetted area is clearly observed. The inter-ELM wetted area is almost constant for the three TF ripple values in the scan, we therefore observe a decrease of ELM power broadening with TF ripple increase and decreasing ELM size. Preliminary analysis of the ELM wetted area for discharges with different ELM sizes but with fixed natural TF ripple show a similar trend of increasing ELM broadening with increasing ELM size. We note here, that the small compound-phase ELMs of the natural TF ripple discharge fall in the same range of the ELM wetted area like the regular type-I ELMs for the $\delta_{\mathrm{BT}} = 0.75\,\%$ discharge (c.f. Fig. 4). The distinction of the ELM size from the TF ripple effects on the ELM wetted area and ELM peak power on the divertor targets requires more analysis of reference discharges. In summary, we find favorable effects of increasing TF ripple, the reduction of ELM size and reduced peak power, but the situation for the plasma facing components are not necessarily relaxed, since the ELM energy reaching the target increases and the ELM wetted area decreases, thereby keeping the ELM associated peak heat flux roughly constant.

This work, supported by the European Communities under the contract of Association between EURATOM/IPP, was carried out within the framework of the European Fusion Development Agreement. The views and opinions expressed herein do not necessarily reflect those of the European Commission.

References

[1] G. Saibene et al., IAEA Proceedings (2008).
[2] N. Oyama et al., J. Physics: Conference Series **123** (2008).
[3] A. Herrmann et al., Plasma Phys. Control. Fusion **37** (1995).
[4] A. Herrmann et al., Europhys. Conf. Abstr. **25** (2001).
[5] P. Andrew et al., J. Nuclear Materials **313-316** (2003).
[6] A. Loarte et al., Phys. Plasmas **11** (2004).
[7] T. Eich et al., Plasma Phys. Control. Fusion **49** (2007).